Polymers, Fractals, and Ceramic Materials

DALE W. SCHAEFER

Concepts borrowed from polymer science have been applied to tailor the properties of inorganic materials, especially those derived from amorphous precursors. Fractal geometry can be used to characterize macromolecular precursors and to relate their structures to kinetic growth processes. Within the silica system, for example, it is possible to manipulate the conditions of solution polymerization to yield a variety of macromolecules from branched chains to smooth colloidal particles.

CERAMIC MATERIALS ARE TRADITIONALLY FABRICATED BY compacting and firing a colloidal powder. The characteristics of the powder (uniformity, homogeneity, and so forth) are critically important to the integrity of the final part, which explains why colloid physics is important in the development of powder processing.

Because powder processing offers limited flexibility, ceramists have long sought new synthetic routes to refractory materials. The sol-gel method, in which an intermediate phase is a gelatin-like solid, is such an alternative. The important concepts underlying sol-gel methods, however, are best understood through insights borrowed from polymer rather than colloid science. It is now becoming clear that the richness of polymer chemistry can be exploited to tailor the properties of inorganic materials in a manner analogous to the development of organic systems. The purpose of this article is to demonstrate the existence of polymeric macromolecules in solution precursors to inorganic materials and to use fractal analysis in conjunction with kinetic growth models and small-angle scattering (SAS) to establish the essential factors that determine the structure of these macromolecules.

Although solution methods are feasible for glasses (amorphous), ceramics (polycrystalline), and glass-ceramics (crystals in an amorphous matrix), sol-gel research has focused on silicate precursors to glasses. At present, these materials find application primarily as optical coatings and aerogels. Aerogels (*1*), which are diaphanous porous solids prepared by drying gels above the critical point of the solvent, are used as Cherenkov radiation detectors in nuclear reactors. Aerogels are also on the verge of commercialization as insulating glazing materials. Solution processing is under development for a variety of applications such as ceramic superconductors, where intimate mixing of the precursor oxides is sought, and electronic materials, where low-temperature processing and high purity are desirable.

Solution processing involves a variety of intermediates or precursors, some of which are depicted in Fig. 1. Depending on reaction conditions, monomers such as $Si(OCH_3)_4$ (tetramethylorthosilicate, TMOS), $Si(OC_2H_5)_4$ (tetraethylorthosilicate, TEOS), or Na_2SiO_3 (sodium metasilicate) can condense to yield a variety of silica (SiO_2) macromolecules.

Generation of silica from solution involves the hydrolysis of alkoxides such as TMOS,

$$Si(OCH_3)_4 + 4H_2O \rightarrow Si(OH)_4 + 4CH_3OH \qquad (1)$$

or sodium metasilicate,

$$Na_2SiO_3{\cdot}H_2O + 2HCl \rightarrow Si(OH)_4 + 2NaCl \qquad (2)$$

Silicic acid, $Si(OH)_4$, then condenses to yield SiO_2,

$$n\,Si(OH)_4 \rightarrow (SiO_2)_n + 2nH_2O \qquad (3)$$

where $(SiO_2)_n$ is a silica macromolecule of as yet unspecified structure.

Fractal geometry (*2*), kinetic growth models (*3–5*), and SAS techniques (*6, 7*) have played key roles in the elucidation of solution precursors. To successfully follow the link between models and structure, one must first understand these concepts.

Fractal Geometry

Fractal geometry is a natural description for disordered objects ranging from macromolecules to the earth's surface (*2*). Figure 2, for example, shows disordered objects that result from simulation of the kinetic models alluded to above. These objects often display "dilation symmetry," which means that they look geometrically self-similar under transformation of scale such as changing the magnification of a microscope.

Structures like those in Fig. 2 can be simply characterized with the single parameter D, the fractal dimension, which is defined as the exponent that relates the mass M of an object to its size R,

$$M \sim R^D \qquad (4)$$

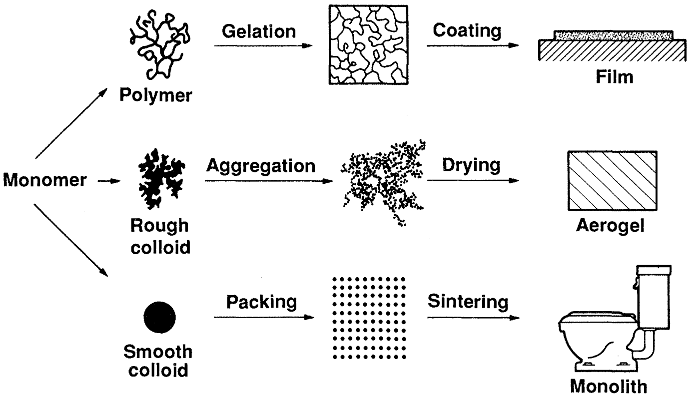

Fig. 1. Ceramic products and precursors.

The author is at Sandia National Laboratories, Albuquerque, NM 87185.

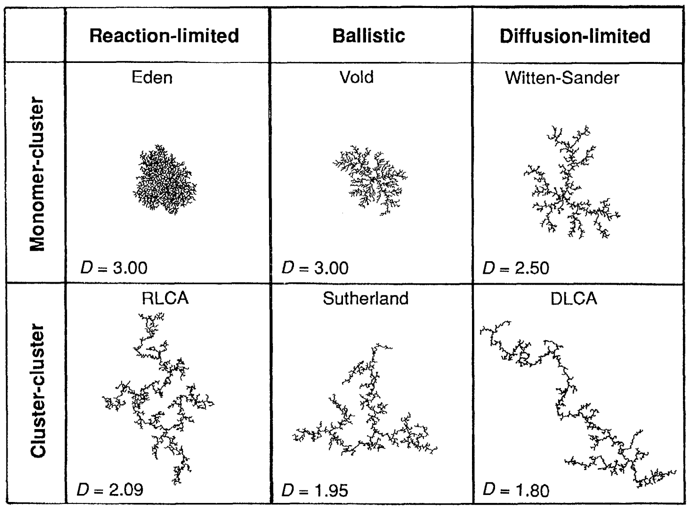

Fig. 2. Kinetic growth models in a 2-D embedding space. Common names for the models as well as the mass fractal dimension D of their 3-D analogs are given. (Courtesy P. Meakin.)

Equation 4 also applies to normal Euclidian objects such as rods, disks, and spheres, for which the exponent D is equal to 1, 2, and 3, respectively, consistent with the common notion of dimensionality. For fractal objects, however, the exponent need not be integral.

Objects described by Eq. 4 are called "mass fractals" or polymers. By contrast, "surface fractals" are uniformly dense (that is, colloidal, $D = 3$, as opposed to polymeric) but have a rough surface. Surface fractals share the self-similarity property, however, in the sense that if the surface is magnified, its geometric features do not change. Mathematically, surface self-similarity is represented by an analog of Eq. 4,

$$S \sim R^{D_s} \tag{5}$$

where S is the surface area and D_s is the surface fractal dimension. For a smooth object, $D_s = 2$, consistent with the notion that a smooth surface is two-dimensional (2-D). For fractally rough surfaces, however, D_s varies between 2 and 3, so D_s is a measure of roughness. The Vold cluster in Fig. 2 is a surface fractal.

Small-Angle Scattering

Fractals can be characterized by scattering techniques. An incident beam (light, neutrons, or x-rays) impinges on a sample, and the angular dependence of the scattered intensity is measured. For fractal objects, the intensity profile has a power-law (*6, 7*) dependence when plotted versus the magnitude of the wave vector K,

$$I \sim K^{-2D+D_s} \tag{6}$$

The quantity $P = -2D + D_s$ is called the Porod slope. Through Bragg's law, the parameter K can be related to a characteristic length L and the scattering angle θ ($K = 2\pi/L = 4\pi\lambda^{-1}\sin\theta/2$), where λ is wavelength. By scanning θ, one effectively studies an object on different length scales determined by K^{-1}. With a combination of light, x-ray, and neutron scattering, it is possible to probe scales between 1 Å and 1 μm.

Although one must be cognizant of exceptions to general rules (*6*), it is usually possible to distinguish structures by the exponent in Eq. 6. Polymeric (mass fractals where $D_s = D$) precursors yield scattering curves with slopes between -1 and -3, whereas smooth colloids give slopes of -4. Rough colloids give slopes (*8*) between -3 and -4.

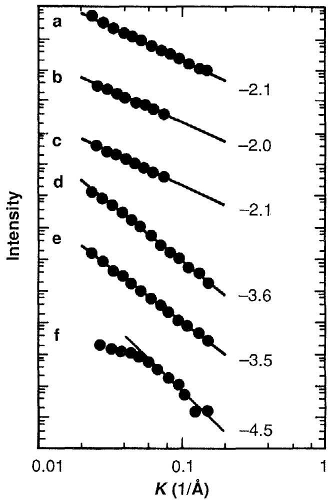

Fig. 3. Small-angle x-ray scattering curves for alkoxides polymerized under a variety of conditions: curve a, TMOS, acid-catalyzed; curve b, TEOS, two-stage, first acid and then base (*13*); curve c, TEOS, two-stage, both acid (*13*); curve d, 1.6*M* TEOS, 0.01*N* NaOH, $W = 4$; curve e, 1.6*M* TMOS, 0.01*N* NaOH, $W = 4$; curve f, 0.2% $Si(OH)_4$ polymerized (*31*) at *p*H = 8.5.

Occasionally, Porod slopes steeper than -4 are observed corresponding to $D_s < 2$ in Eq. 6. Schaefer *et al.* have observed this behavior in surfactant-coated colloidal particles (*9*) and have referred to these layers as "subfractal" interfaces. The value $D_s < 2$ corresponds to surface roughness whose amplitude diminishes with distance (along or perpendicular to the surface) in a power-law fashion. It is not clear why interfacial layers follow this description.

The analysis of the Porod slopes of SAS curves is illustrated in Fig. 3, which shows data on silicate systems polymerized under a variety of conditions. The conditions differ in catalysis (acid versus base), polymerization protocol (single-stage versus two-stage), water/silicon ratio W, and monomer constitution [TMOS, TEOS, or $Si(OH)_4$]. The data show that polymers are produced under acid catalysis, two-stage polymerization, and low W. Colloidal particles, with rough or smooth surfaces, are produced with base catalysis when W is about 4. The purpose of the rest of this article is to understand why these structures are realized. To accomplish this goal it is useful to map the polymerization processes onto kinetic growth models.

Kinetic Versus Thermodynamic Models

Kinetic growth models (Fig. 2) describe polymerization and aggregation processes that occur far from equilibrium. In chemical systems, these models are realized when unions between growing species are strong and irreversible; that is, for bonds that, once formed, do not dissociate. These models are reasonable for silica because the Si–O–Si linkage is very strong and does not dissociate except under quite basic conditions.

Other models describe growth close to equilibrium, such as spinodal decomposition or nucleation, and growth. Neither of these thermodynamic models is expected to produce polymeric structures, which explains the dominance of the colloidal perspective in the solution processing of ceramics.

Although in 1955 Bechtold (*10*) provided evidence for the existence of chain-like structures in silica solutions, Iler's influential book (*11*) took a disparaging view of concepts borrowed from organic polymer chemistry. It was Sakka and Kamiya's demonstration (*12*) that fibers could be pulled from silica solutions, together with scattering studies by Schaefer and Keefer (*13*), that forced a reevaluation of the applicability of polymer concepts to soluble silicates.

With scattering techniques it is possible to settle the dispute

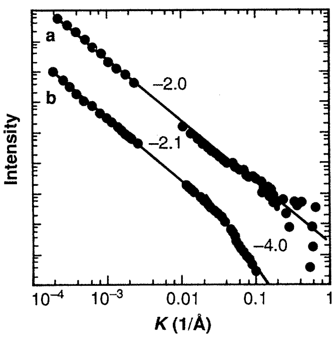

Fig. 4. Contrasting SAXS profiles for (a) polymeric and (b) colloidal systems. Profile a is from a rapidly neutralized 0.2% sodium metasilicate solution in water (*31*), profile b from a rapidly neutralized water suspension of colloidal silica (*14*).

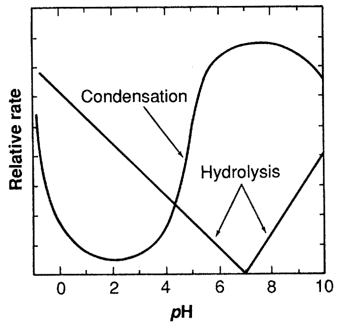

Fig. 5. Schematic comparison of the rates of hydrolysis and condensation in silicates. The layout is Keefer's analysis (*20*) based on a variety of results (*11, 32, 33*).

between the polymeric and colloidal viewpoints. In the conventional view, polymerization proceeds by accretion on particulate nuclei. Depending on *p*H, these nuclei grow to larger particles or aggregate into ramified (now we say fractal) clusters (or both).

If the nucleation model is correct, the late-stage scattering profile will display a Porod slope of -4 for $Ka > 1$ (a is the size of the primary colloidal particles) and will display a slope between -1 and -3 for $Ka < 1$, depending on the structure of the aggregate. Indeed, this profile is observed for aggregates of colloidal particles (*14*) (Fig. 4, curve b). With the definitions given above, the scattering data in Fig. 4, curve b, for colloidal aggregates show that this system is nonfractal and smooth on length scales below 100 Å, the primary particle size, and is mass-fractal on larger scales.

The scattering curve for the colloidal system contrasts with that observed when Na_2SiO_3 is abruptly neutralized to $Si(OH)_4$. This scattering profile (Fig. 4, curve a) shows no transition at large K, demonstrating that this system is polymeric down to molecular dimensions. Because the Porod slopes are the same for both systems for $K < 0.01$ $Å^{-1}$, we can reasonably conclude that the structures are similar on length scales greater than 100 Å. In a sense, even the colloidal aggregate (curve b) is a polymer, the monomers being the 100 Å primary particles. Clearly, polymers have a great deal to do with silica solutions. Kinetic models provide the link between polymers and silica chemistry.

Kinetic Growth Models

The kinetic models illustrated in Fig. 2 are distinguished by assumptions concerning mass transport and accretion. Mass transport refers to the process by which reacting molecules approach each other. If the transport is Brownian, the process is diffusion-limited (*3, 4*) and falls in column 3 of the figure. In this limit, growth occurs primarily at the tips of the cluster and the process is termed diffusion-limited cluster aggregation (DLCA). In the reaction-limited process (RLCA) (*5, 15*) transport plays no role at all, so all available sites are equal targets for accretion, leading to more compact clusters (column 1 of the figure). The intermediate case is ballistic aggregation (*16*), which describes the growth of clusters that approach each other along linear trajectories. I described applications of these models in a previous review (7). Silica polymerization falls into the reaction-limited regime: bond formation is an activated process, so growth is related to crossing a potential barrier and is independent of transport.

Kinetic models are also distinguished by assumptions concerning accretion. When the dominant growth process occurs by the addition of small species to large clusters, we have monomer-cluster (MC) growth. By contrast, cluster-cluster (CC) growth describes the limit in which clusters of all sizes can bond. In the reaction limit, MC growth yields colloidal particles whereas CC growth yields polymers.

Polymers and Reaction-Limited Cluster Aggregation

Both systems in Fig. 4 exhibit RLCA. When $Si(OH)_4$ is generated abruptly by reduction of the *p*H of a Na_2SiO_3 solution (curve a), a burst of reactive monomers [$Si(OH)_4$] is produced far from equilibrium. Condensation reactions occur at random, leading directly to RLCA polymers with $D \simeq 2$. Similarly, if a colloidal solution is destabilized (curve b), the particles suddenly find themselves far from equilibrium and proceed to aggregate by RLCA. RLCA is usually realized whenever random condensation or aggregation of preexisting reactive species occurs far from equilibrium.

Polymers are also produced from alkoxides, but now hydrolysis, Eq. 1, takes on an important role (*7, 9, 17*). Figure 5, which schematically shows the relative rates of hydrolysis and condensation in alcohol, helps to identify the conditions for RLCA. When the hydrolysis reaction is fast compared to condensation (*p*H 2 to 5), a burst of reactive monomers is generated and these monomers proceed to condense at random, leading to RLCA. Figure 3, curve a, shows data for the acid-catalyzed TMOS polymerization giving the RLCA slope of -2.1. Other acid-catalyzed alkoxides often are more compact on short scales (*17*), perhaps because of an initial tendency toward a more compact growth habit. For length scales beyond 100 Å, however, slopes near -2 appear to be the norm.

Polymers are also observed if alkoxide polymerization is carried out in two steps (*17, 18*). Because monomers are largely exhausted in the first stage of the reaction, second-stage polymerization proceeds by CC growth regardless of catalytic conditions. Indeed, the late-stage structure (on length scales exceeding 10 Å) of silicates produced under two-stage polymerization is nearly independent of *p*H in the second stage, consistent with the mapping onto RLCA (*7, 17*). The similarity of curves b and c in Fig. 3 supports this contention.

Colloids and Eden Growth

Eden-like or reaction-limited MC growth is expected under basic conditions (*17, 19*) whereas CC reactions are discouraged by the nucleophilic condensation mechanism, which requires inversion of one of the reacting species (*20*). Figure 3, curve f, shows data for $Si(OH)_4$ polymerized at $pH = 8.5$, the highest *p*H at which silica is insoluble. Although colloids are found (that is, the Porod slope is less than -3), the measured slope of -4.5 implies a subfractally rough surface, a characteristic not yet identified in the Eden model simulations.

Base-catalyzed TEOS also polymerizes by MC growth. Hydrolyzed monomers are generated slowly but condense rapidly (Fig. 5) thus exhibiting a tendency toward the MC regime (*9*). The polymerizing species, however, is a substituted silicic acid, $Si(OR)_{4-x}(OH)_x$, so the Eden model must be replaced by a modification that Keefer and Schaefer called "poisoned Eden" (PE) growth (*19*). Growth takes place by a MC process, but a fraction $4 - x$ of the monomer bonds are nearly unreactive toward condensation, corresponding to unhydrolyzed sites on the monomer. Depending on the degree of poisoning, a variety of structures are realized, from linear polymers to dense particles. Fractally rough clusters result from PE growth when there is a very broad distribution (*21*) in monomer functionality, x. The base-catalyzed TEOS data (Fig. 3, curve d) are consistent with PE growth.

For TMOS, the conditions assumed above for PE growth break down even under base catalysis. In contrast to TEOS, where hydrolysis of condensed clusters is impeded (*22*), hydrolysis in TMOS is random, occurring equally on both monomers and condensed clusters (*23*). It is not surprising, therefore, that some striking differences are observed. The most notable difference is that base-catalyzed TMOS solutions gel, whereas base-catalyzed TEOS solutions do not. TMOS polymerization can be understood by modeling cluster rather than monomer hydrolysis.

Kinetic Percolation

Because TMOS hydrolysis is purely statistical (*23*), growth is limited by hydrolysis on the cluster, leading to a growth process that might be called kinetic percolation (KP) because of an analogy with an algorithm for generating percolation clusters developed by Leath (*24*). On a computer, percolation clusters (*25*) are formed by randomly filling sites on a lattice, like raindrops falling on a surface. In Leath's algorithm, however, clusters are "grown" starting from a seed site with random occupation of sites neighboring the seed. Only a fraction P of sites are randomly selected. Further generations are similarly added on an ever-increasing perimeter. The seed cluster will always die (that is, at some generation no perimeter sites are selected) if P is below the percolation threshold P_c. Above P_c, however, there is a finite probability that every generation will survive, so growth occasionally proceeds without limit. KP describes CC growth that is limited by hydrolysis on the cluster.

The threshold percolation cluster is critically branched. Clusters with more or less branching have a fundamentally different geometry. Alexandrowicz (*26*) showed that percolation clusters can also be grown by a MC process called a branched self-avoiding walk, a model analogous to the self-avoiding walk for linear polymers.

If KP describes TMOS polymerization, then the growing clusters should have the topology and fractal dimension of the infinite percolation cluster ($D = 2.5$). If D is below 2.5, growth eventually ceases. If D exceeds 2.5, growth is outside the hydrolysis limit and uniformly dense clusters (*27*) corresponding to $P > P_c$, are expected. The situation where there is just sufficient hydrolysis to sustain growth should lead to critical branching.

Figure 6 supports the KP model for TMOS polymerization at $pH = 7$, where the system is strongly hydrolysis-limited. For $W \leq 4$, the scattering curves are independent of W with a slope of $\simeq -2.5$ consistent with critical branching. The stoichiometric value for Eqs. 1 through 3 is $W = 2$. Below P_c the slope is -2.1, approaching the "lattice animal" fractal dimension ($D = 2.0$) found in percolation well below threshold (*25*).

At both higher and lower *p*H, the extreme hydrolysis-limited situation breaks down. Under more basic conditions, growth is not limited by cluster hydrolysis and the system is forced above threshold where fractally rough clusters are observed (Fig. 3, curve e), as expected in both the KP and the PE models (PE is equivalent to KP if the functionality distribution is appropriately weighted). At lower *p*H the system becomes increasingly condensation-limited, leading to RLCA (Fig. 3, curve a).

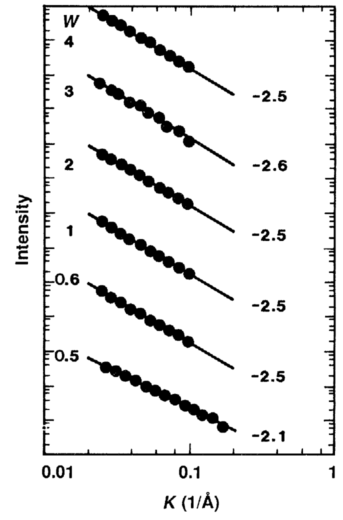

Fig. 6. SAXS profiles for $1.6M$ TMOS polymerized at $pH = 7$ as a function of $W = [H_2O]/[Si]$. Slopes of -2.5, characteristic of the spanning cluster in percolation theory, are in the hydrolysis-limited regime above threshold. Slopes should approach 2.0, the lattice animal result, well below P_c. P_c is calculated to correspond to $W = 0.77$, although empirically the system gels above $W = 0.5$.

Strictly speaking, percolation implies a particular cluster mass distribution (*25*). In the kinetic perversion proposed here, however, percolation topology results in the absence of the equilibrium distribution of cluster sizes. It should also be emphasized that many clusters develop simultaneously. The emphasis on a single threshold cluster is strictly pedagogical. Finally, systems that develop by a MC accretion eventually display a crossover to another growth habit as the monomers are exhausted. On large length scales, all kinetic systems become ramified (*17*). Indeed, a host of recent experimental results show striking universality near the gel point of a variety of polymerizing systems.

Nucleation and Growth

Under strongly basic conditions, SiO_2 is increasingly soluble and growth of the particles is dictated by thermodynamics rather than kinetics. Indeed, Keefer (*20*) studied the evolution of small-angle x-ray scattering (SAXS) curves for fractally rough TEOS clusters in $0.01M$ ammonium hydroxide (NH_4OH). On long time scales, he observed progressive steepening of the SAXS profile, consistent with the smoothing of the surface of the colloidal particles. In this case, the early growth is kinetic but late-stage development is near equilibrium.

Fully dense, smooth spherical colloidal particles are synthesized by polymerization close to equilibrium where thermodynamic models apply. Commercial colloidal silica (like that used in Fig. 4, curve b) is prepared by slowly reducing the *p*H of a concentrated sodium metasilicate solution by ion exchange or electrodialysis. Silica is quite soluble under typical conditions leading to conventional nucleation and growth. In the so-called Stöber (*28*) process, alkoxides are polymerized under exceedingly basic conditions where high solubility and complete hydrolysis guarantee nucleation and growth. Nucleation and growth may occur faster than kinetically limited growth. The essential difference is related to the reversible nature of bond formation under strongly basic conditions.

Applications

Kinetic models provide a framework within which process engineers can manipulate precursor growth conditions to achieve particular structural goals. As implied by Fig. 1, different applications require different precursors. Acid-catalyzed alkoxides form dense films that sinter at relatively low temperature (*29*). If porous films, on the other hand, are desired for index-matched coatings, then base-catalyzed materials (even colloidal particles) provide the required rigidity necessary to achieve porous films with tailorable refractive index (*30*).

For the preparation of bulk monoliths, other considerations apply. Although acid catalysis leads to relatively dense solids, these do not sinter well because closed porosity precludes the escape of organics. The local rigidity afforded by base-catalyzed systems, however, allows sufficient open porosity to effectively sinter bulk monoliths. These examples show that kinetic models are useful, not only for explaining existing data on the structure and processibility of sol-gel–derived materials, but also as a framework for the control variables that can be manipulated to achieve particular structural and processing goals.

REFERENCES AND NOTES

1. J. Fricke, *Sci. Am.* **258**, 92 (May 1988).
2. B. B. Mandelbrot, *The Fractal Geometry of Nature* (Freeman, San Francisco, 1982).
3. T. A. Witten and M. E. Cates, *Science* **232**, 1607 (1986).
4. L. M. Sander, *Sci. Am.* **256**, 94 (January 1987).
5. P. Meakin, *Adv. Colloid Interface Sci.* **28**, 249 (1989).
6. J. E. Martin and A. J. Hurd, *J. Appl. Crystallogr.* **20**, 61 (1987).
7. D. W. Schaefer, *Mater. Res. Soc. Bull.* **13-2**, 22 (1988).
8. H. D. Bale and P. W. Schmidt, *Phys. Rev. Lett.* **53**, 596 (1984).
9. D. W. Schaefer *et al.*, in *Physics and Chemistry of Porous Media II*, J. R. Banavar, J. Koplik, K. W. Winkler, Eds. (American Institute of Physics Conference Proceedings, New York, 1987), vol. 154, pp. 63–80.
10. M. F. Bechtold, *J. Phys. Chem.* **59**, 532 (1955).
11. R. K. Iler, *The Chemistry of Silica* (Wiley-Interscience, New York, 1979), pp. 117–172.
12. S. Sakka and K. Kamiya, *J. Non.-Cryst. Solids* **48**, 31 (1982).
13. D. W. Schaefer and K. D. Keefer, *Phys. Rev. Lett.* **53**, 1383 (1984).
14. D. W. Schaefer, J. E. Martin, P. Wiltzius, D. S. Cannell, *ibid.* **52**, 2371 (1984).
15. M. Kolb, R. Botet, R. Jullien, *ibid.* **51**, 1123 (1983).
16. D. Bensimon, E. Domany, A. Aharony, *ibid.*, p. 1394.
17. D. W. Schaefer and K. D. Keefer, *Mater. Res. Soc. Symp. Proc.* **73**, 277 (1986).
18. C. J. Brinker, K. D. Keefer, D. W. Schaefer, C. S. Ashley, *J. Non-Cryst. Solids* **48**, 47 (1982).
19. K. D. Keefer and D. W. Schaefer, *Phys. Rev. Lett.* **56**, 2376 (1986).
20. K. D. Keefer, *Mater. Res. Soc. Symp. Proc.* **32**, 15 (1984).
21. ——, *ibid.* **73**, 295 (1986).
22. J. C. Pouxviel and J. P. Boilot, *ibid.* **121**, 37 (1986).
23. R. A. Assink and B. D. Kay, *ibid.* **32**, 301 (1986).
24. P. L. Leath, *Phys. Rev. B* **14**, 5046 (1976).
25. D. Stauffer, *Introduction to Percolation Theory* (Taylor and Francis, London, 1985).
26. Z. Alexandrowicz, *Phys. Lett. A* **80**, 284 (1980).
27. R. F. Voss, *J. Phys. A* **17**, L373 (1984).
28. W. Stöber, A. Fink, E. Bohn, *J. Colloid Interface Sci.* **26**, 62 (1968).
29. M. Nogami and Y. Moriya, *J. Non-Cryst. Solids* **37**, 191 (1980).
30. C. J. Brinker, in *Ultrastructure Processing of Advanced Ceramics*, J. K. MacKenzie and D. R. Ulrich, Eds. (Wiley, New York, 1988), pp. 223–240.
31. D. W. Schaefer, A. J. Hurd, J. E. Martin, A. Glines, in preparation.
32. R. Aelion and F. Eirich, *J. Am. Chem. Soc.* **72**, 5705 (1950).
33. C. Okkerse, in *Physical and Chemical Aspects of Adsorbents and Catalysts*, G. G. Linsen, J. M. H. Fortuin, C. Okkerse, J. J. Steggerda, Eds. (Academic Press, New York, 1970), pp. 213–264.
34. I thank K. Keefer for extensive education in silica chemistry and P. Meakin for the simulated clusters in Fig. 2. This work, performed at Sandia National Laboratories, Albuquerque, NM, was supported by U.S. Department of Energy contract DE-AC-04-76DP00789 for the Office of Basic Energy Sciences, Division of Materials Science.

Genetic Control of Differentiation of the *Caenorhabditis elegans* Touch Receptor Neurons

MARTIN CHALFIE AND MACY AU*

The genetic control of neuronal differentiation has been studied by examining mutations that affect the development and function of the six touch receptor neurons of the nematode *Caenorhabditis elegans*. By screening for touch-insensitive mutants, it has been possible to identify 18 genes (represented by 417 mutations) that are required at various stages in the developmental program for touch cell differentiation. Two of the genes are needed for the generation of precursors in the touch cell lineages; without the precursors, touch cells are not made. A third gene, *mec-3*, specifies the differentiation of the touch cells, probably by acting as a transcription factor. The remaining 15 genes are likely targets of *mec-3* action; mutants defective in these genes have nonfunctioning, yet differentiated, touch cells. Some of these latter genes are needed for the formation of cell-specific components of the touch cells, such as a set of microtubules that are only found in these cells. The study of the touch genes should help us understand how touch cell fate is determined, how microtubule form is specified, and, perhaps, how mechanical stimuli are transduced.

NERVOUS SYSTEMS CONSIST OF MANY TYPES OF NEURONS that differ from each other structurally and biochemically in such features as shape, patterns of connectivity, neurotransmitters, receptors, and channels. Considerable diversity is seen even in organisms with relatively few neurons. For example, the 302 nerve cells of the nematode *Caenorhabditis elegans* have been classified into 118 groups (*1*). The mechanism by which cells attain their individual, differentiated features is not known; cell-cell interactions, growth factors, and intrinsic determinants are all thought to influence the expression of cell-specific characteristics.

One method of studying the control of the differentiation of

The authors are in the Department of Biological Sciences, Columbia University, New York, NY 10027.

*Present address: Department of Pharmacology, New York University Medical School, New York, NY 10016.